*Chapter 6*

# Synthesis and Characterization of CIT-13

Contents of this chapter were obtained in collaboration with Dr. Dan Xie and Dr. Stacey I. Zones from Chevron Energy Technology Company, Dr. Stef Smeets and Prof. Lynne B. McCusker from ETH Zurich and Stockholm University. Dr. Smeets and Prof. McCusker collected synchrotron XRD data and refined the structure of CIT-13. A part of the results and discussions of this chapter was published on August 18th, 2016: J. H. Kang et al., *Chem. Mater.* 2016, **28**, 6250, DOI: 10.1021/acs.chemmater.6b02468.

## 6.1. Introduction

The synthesis of a zeolite is one of the most complicated chemical assemblies, and involves control of various synthetic parameters such as pH, water content, structures of OSDA, types of alkali cations, mineralizing agents, aging time, etc.[131, 168] Zeolite synthesis has traditionally been regarded as a delicate art which inevitably entails a number of trials and errors.[117, 169] Synthesis of extra-large-pore molecular sieves is particularly challenging due to the low framework density of the desired structures. Corma et al. suggested several strategies to obtain extra-large-pore molecular sieves such as the use of rigid three-dimensional OSDAs, the use of fluorides which helps to lower the framework density, the use of high-throughput gel-composition screening systems, etc.[114] Although there is no proven road to the discovery of novel extra-large-pore frameworks, inclusion of germanium in the system together with fluoride as the mineralizing agent can be a good starting point

since both germanium and fluoride favor the formation of composite building units such as *d*4*r* units consisting of small-rings which is beneficial to lower the framework density.[116, 149]

One of the classes of OSDAs having rigid structures is the imidazolium-derived cations. Imidazole-based OSDAs are potential candidates that can probably yield extra-large-pore frameworks thanks to their rigid structures and ability to have the π-π interactions.[114] In the course of testing various methylbenzylimidazolium-derivatives in the germanosilicate system with fluoride, our group discovered a new extra-large-pore germanosilicate named CIT-13.[63] The structure of CIT-13, solved on the basis of RED technique, showed an impressive resemblance to an UTL-type germanosilicate IM-12 which has been extensively studied in terms of its ability to undergo topotactic transformations.

In this chapter, the optimized synthesis condition for germanosilicate CIT-13 will be provided by testing the influences of each synthetic parameters such as types of OSDAs, germanium content, water content, crystallization temperature, etc. Also, several other synthetic protocols such as the hydroxide-mediated synthesis and the isomorphous substitution of aluminum in germanosilicate synthesis will be introduced. On the basis of the refined structure solution of CIT-13, the nature of possible disorders in the framework will be discussed. Lastly, the physicochemical properties of resultant molecular sieves will be characterized and discussed.

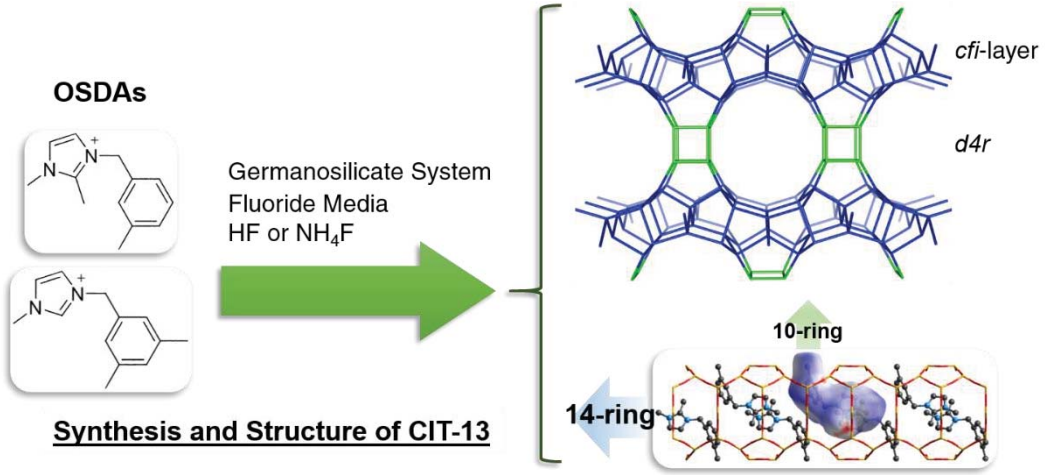


Figure 6.1. Brief graphic description of synthesis and structure of germanosilicate CIT-13. Reproduced with Permission from Ref [170]. Copyright 2014 American Chemical Society.

## 6.2. Experimental

### 6.2.1. Synthesis of OSDAs

All OSDAs used in this work were prepared from the cross-$S_N2$ reactions between two imidazole-derivatives and two methylbenzyl or dimethylbenzyl halides. 1,2-dimethylimidazole (98%), 1-methylimidazole (98%), 3-methylbenzyl chloride (98%) were purchased from Sigma-Aldrich. 3,5-dimethylbenzyl bromide (98%) was purchased from Alfa Aesar. All chemicals were used without further purification steps. In this chapter, the following four organic cation OSDAs were used to synthesize CIT-13: (**1**) 1,2-dimethyl-3-(3-methylbenzyl)imidazolium, (**2**) 1,2-dimethyl-3-(3,5-dimethylbenzyl)imidazolium, (**3**) 1-methyl-3-(3-methylbenzyl)imidazolium, (**4**) 1-methyl-3-(3,5-dimethylbenzyl)imidazolium. The schemes for the preparations of these OSDAs were illustrated in Figure 6.2.

150 mmol of imidazole-derivative (i or ii) was firstly dissolved in 500 ml of toluene. Then, an equimolar amount of benzyl halide-derivative (iii or iv) was added slowly. In the

case of the addition of 3,5-dimethylbenzyl bromide, the reaction which is exothermic underwent quickly even at room temperature due to the good ability of bromide as the leaving group of the substitution reaction. Therefore, the addition of 3,5-dimethylbenzyl bromide should be performed gradually in an ice bath. The reaction mixture was heated up to 105 °C and stirred for 1 day. Since the product salt is insoluble in toluene, the mixture became cloudy after several hours and the sedimentation of the powdery product phase was observed after 24 hours. The batch was cooled down, and this solid product was recovered by filtration. The product was washed using a copious amount of diethyl ether repeatedly and dried overnight in a vacuum at room temperature. One more OSDA denoted as "Ortho" in Table B4 is 1,2-dimethyl-3-(2-methylbenzyl)imidazolium which is the ortho-isomer of OSDA 1. This OSDA was synthesized in an analogous way.

Another OSDA, (6R,10S)-6,10-dimethyl-5-azaspiro[4.5]decanium (Figure 6.3.) was also synthesized to prepare IM-12 germanosilicates which was compared to CIT-13.[116] 1 M NaOH aqueous solution (160 ml) was mixed with 150 mmol of 1,4-dibromobutane in a 500-ml double-neck round-bottom flask. The mixture was heated up to the reflux under vigorous stirring. 150 mmol of cis-2,6-dimethylpiperidine was added gradually for 45 min to eliminate the possibility of dimer formation. The reaction mixture was refluxed overnight. Using a dry-ice bath, the batch was cooled down. A portion of concentrated NaOH solution (50 wt.% in $H_2O$) was added until a floating brownish second phase appeared. An extended cooling made this oil phase solidify. This solid phase was filtered, and extracted with 200 ml of chloroform three times. The extracted chloroform phase can be dark and murky due to the presence of moisture. This mixture was dried with anhydrous magnesium sulfate. The clear solution was separated by filtration. Excess chloroform was removed by evaporation using a rotary evaporator. The solid was recovered and recrystallized with a small portion of chloroform (100 ml) and diethyl ether. This solid product was recovered by filtration. The product was washed using a copious amount of diethyl ether repeatedly and dried overnight in a vacuum at room temperature.

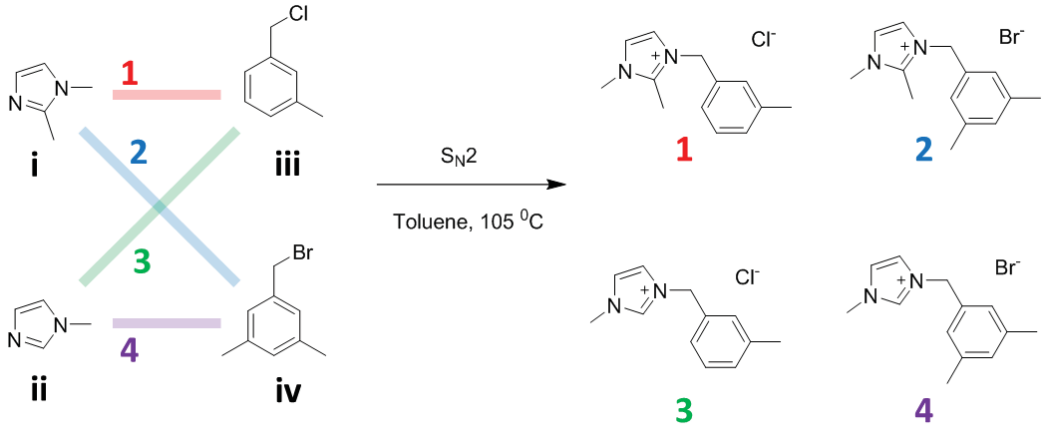


Figure 6.2. Reactions schemes for the syntheses of the OSDAs used in this work and the structures of them: i. 1,2-dimethylimidazole, ii. 1-methylimidazole, iii. 3-methylbenzyl chloride, iv. 3,5-dimethylbenzyl bromide, 1. 1,2-dimethyl-3-(3-methylbenzyl)imidazolium, 2. 1,2-dimethyl-3-(3,5-dimethylbenzyl)imidazolium, 3. 1-methyl-3-(3-methylbenzyl)imidazolium, 4. 1-methyl-3-(3,5-dimethylbenzyl)imidazolium

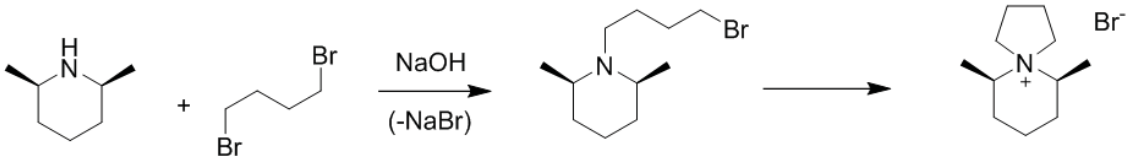


Figure 6.3. Reaction scheme for the synthesis of (6R,10S)-6,10-dimethyl-5-azaspiro[4.5]decanium.

To prepare OSDA hydroxide aqueous solutions which were used to prepare germanosilicate gels, ion-exchange steps were conducted. The product organic salts were dissolved in distilled water first (ratio: 500 ml of water per 100 mmol of product). Next, ion-

exchange resin (Dowex™ Monosphere™ 550A Hydroxide Form, Dow Chemical) was added to the solution (ratio: 300 ml (in volume) of ion-exchange resin per 100 mmol of product). The ion-exchange mixture was stirred at room temperature for 1 day. The solution phase was recovered by filtering out the resin. The same amount of resin was added again to the solution, and an exchange step was repeated for an extra day. After that, the solution phase was concentrated using a rotary evaporator until the solution volume became 100 to 200 ml. The concentration of the final OSDA hydroxide solution was characterized based on acid-base titration using a Mettler Toledo DL22 titrator. The desired concentration of the final solutions was 0.2–2 mmol $OH^-$ per gram of solution.

### 6.2.2. Synthesis of Germanosilicates

All germanosilicate molecular sieves were synthesized by hydrothermal reactions. For a typical CIT-13 synthesis in fluoride media, the gel composition was x/(1+x) $SiO_2$ : 1/(1+x) $GeO_2$ : y ROH : y HF (or $NH_4F$) : z $H_2O$, where x is essentially the Si/Ge molar ratio of the gel, and ROH is the desired imidazolium-derivative OSDA hydroxide. The values of x, y and z and synthesis results attempted in this work are provided in Table B1. First, a desired amount of germanium dioxide ($GeO_2$, 99.999%, Strem chemical) was dissolved in OSDA solution in a 23-ml PTFE liner for a Parr steel autoclave. Then, a desired amount of tetraethyl orthosilicate (TEOS, 98%, Alfa Aesar) was added to the mixture and stirred overnight to fully hydrolyze TEOS. Using an air flow, the gel was dried until it became thick and viscous. After that, concentrated hydrogen fluoride (HF, Sigma-Aldrich, 48% in $H_2O$) was added dropwise. (*Caution: Hydrogen fluoride is a dangerous substance that can cause fatal burns and irreversible damages to human skin, tissue, and bone. It must be handled with appropriate PPE including a lab coat, a respirator, a full-face shield, an acid-apron, a pair of long-sleeve nitrile gloves, etc. with a proper ventilation in a fume hood.*) The addition of HF turns clear viscous gel into a powdery phase. If ammonium fluoride ($NH_4F$) was used as the fluoride source, it was added with germanium dioxide. The gel was dried for an extra

couple of days to evaporate the remaining water and ethanol. As the final gel preparation step, a desired amount of water was added to meet the target gel composition. If necessary, the batch was seeded with as-made CIT-13 (5 wt. % with respect to $SiO_2$+$GeO_2$ in the gel). The liner was tightly sealed with a Parr steel autoclave and placed in a 160 °C static oven. An oven designed to agitate the batches by rotating them at 70 rpm was also used. Aliquoting was performed weekly in order to monitor the crystallization progress.

Aluminogermanosilicate CIT-13s were synthesized similarly to the cases of pure germanosilicate CIT-13 described above. For aluminum source, aluminum isopropoxide (98%, Sigma-Aldrich) was used. The ternary gel composition was x $SiO_2$ : y $AlO_{3/2}$ : z $GeO_2$ : 0.5 ROH : 0.5 HF : 10 $H_2O$ where x + y + z = 1. The detailed compositions (x, y, z) are shown in the ternary gel composition diagram illustrated in Figure 6.7(a) shown in the following section. The crystallization was performed in the range of 150–175 °C for 1–4 weeks. Aliquoting was also performed on a weekly basis to monitor the crystallization progress. CIT-13-type aluminogermanosilicates prepared from this protocol were denoted Al/Ge-CIT-13.

The CIT-13 syntheses were also attempted without use of fluoride mineralizers. For a typical CIT-13 synthesis in hydroxide media, the gel composition was x/(1+x) $SiO_2$ : 1/(1+x) $GeO_2$ : 0.5 ROH : y $H_2O$, where x is the Si/Ge molar ratio of the gel, and ROH is the desired imidazolium-derivative OSDA hydroxide. The values of x and y and crystallization conditions attemped in this work are provided in Table B4 with the results. For silicon sources, TEOS and fumed silica (ACROS, Cab-O-Sil®) were used. The general procedure for hydroxide-mediated synthesis was analogous to the cases of fluoride syntheses explained above, except that the addition of HF or $NH_4F$ is omitted. Excess water and ethanol were evaporated using an air flow. During the drying step, the gel weights must be measured very carefully to reliably estimate the water contents. The final gels having desired compositions

were generally translucent and had very sticky textures. It is recommendable to measure the weights of PTFE liners and stirring bars before starting this procedure.

For a typical IM-12 synthesis,[116] a germanosilicate gel having a composition 0.667 $SiO_2$ : 0.333 $GeO_2$ : 0.25 ROH : 30 $H_2O$ was prepared, were ROH is (6R,10S)-6,10-dimethyl-5-azaspiro[4.5]decanium hydroxide. Firstly, a desired amount of fumed silica and germanium dioxide were dispersed in the OSDA solution and homogenized by stirring overnight. After that, a desired amount of water was added or evaporated to make the final gel have the target composition. The mixture was sealed in a Parr autoclave and placed in a 175 °C static oven for 14 days. Similarly, aliquots were taken periodically to monitor the crystallization.

### 6.2.3. Characterization

Powder X-ray diffraction (PXRD) patterns were acquired using a Rigaku MiniFlex II benchtop diffractometer using Cu Kα radiation (λ = 1.54184 Å) to assess the crystal structure and crystallinity of the products. The refined structure of as-prepared CIT-13 was obtained from synchrotron X-ray diffraction data performed at the MS-Powder beamline at the Swiss Light Source in Villigen, Switzerland.

Morphology and elemental composition (Si/Ge molar ratios of germanosilicates) were studied using a Zeiss 1550VP field-emission scanning electron microscope (FE-SEM) equipped with an Oxford X-Max SDD X-ray energy dispersive spectrometer. Pore volumes and pore-size information of microporous materials were studied based on Ar adsorption isotherms obtained using a Quantachrome Autosorb iQ at 87.45 K. Thermogravimetric analyses (TGA) profiles were performed to quantify weight fractions of occluded organic molecules in as-prepared CIT-13s using a PerkinElmer STA 6000 instrument.

$^{1}H$ and $^{13}C$ nuclear magnetic resonance (NMR) spectra of OSDAs were acquired using a Varian 500 MHz spectrometer with carrier frequencies of 499.843 and 125.686 MHz, respectively. $^{1}H$, $^{13}C$, $^{27}Al$ and $^{29}Si$ magic-angle spinning (MAS) solid-state NMR spectra of samples were obtained using a Bruker Avance 500 MHz spectrometer with carrier frequencies of 499.843, 125.686, 130.287 and 99.305 MHz, respectively. A 4-mm zirconia rotor with a Kel-F cap was charged with 50–100 mg of as-made or freshly calcined germanosilicate. The MAS rate was 8 kHz both for $^{1}H$-$^{13}C$ cross-polarization (CP) and normal bloch-decay $^{29}Si$ experiments, and 12 kHz for $^{27}Al$ experiments.

## 6.3. Results and Discussion

### 6.3.1. Effects of Synthetic Parameters

#### *6.3.1.1. Germanosilicate System in Fluoride Media*

The crystallization of germanosilicate CIT-13 was affected by many synthetic parameters. In this work, effects of gel Si/Ge ratios, water contents, OSDA and fluoride contents, type of fluoride source, and crystallization temperatures were systematically studied. Also, the structure-directing abilities of the four OSDAs were investigated. The batch of a gel composition 0.8 $SiO_2$ : 0.2 $GeO_2$ : 0.5 ROH : 0.5 HF : 10 $H_2O$ (OSDA = **1**) crystallized in an 160 °C static oven for 2–3 weeks was designated as *the reference condition*. From this reference condition, pure phase CIT-13 was reproducibly obtained. Each synthetic parameter was studied by varying only that parameter from the reference condition. The results of synthesis trials are summarized in Table B1, and the PXRD profiles from several selected successful synthesis conditions are displayed in Figure 6.4. No remaining $GeO_2$ phase was observed in any conditions.

The Si/Ge ratio of gels made a crucial impact on the formation of CIT-13. Gel Si/Ge ratios within a range from 2 to 16 were studied for OSDA **1**. From gel compositions of Si/Ge ratios 2, 3, and 4 (reference) gave pure CIT-13 phases having crystal Si/Ge ratios 3.84±0.59, 4.72±0.55, and 5.73±0.89, respectively. Si/Ge ratios of resultant CIT-13 crystals were higher than those of mother germanosilicate gels. The correlation of gel Si/Ge ratios to crystal Si/Ge ratio is illustrated in Figure B1. Also, the higher Ge content a gel had, the faster the crystallization of CIT-13 was. When gel Si/Ge ratios were 2 and 3, the crystallization was completed within 2 weeks. The gel having Si/Ge ratio = 4 crystallized after 3 weeks. When Si/Ge > 8, one or more impurity phases started to appear. The PXRD profiles of relevant batches from which aliquots were taken with an interval of 1 week are displayed in Figure B2.

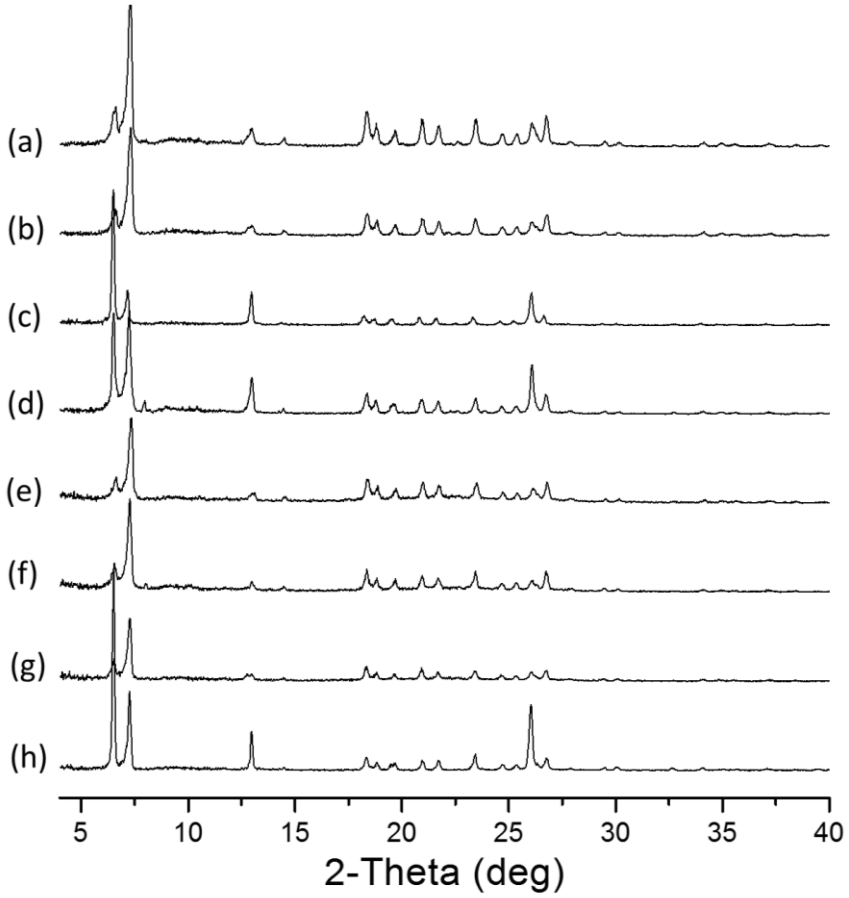


Figure 6.4. PXRD profiles of selected crystallization conditions which gave high-purity CIT-13: (a) reference condition, (b) Si/Ge = 3, (c) seeded, (d) $H_2O/T$ = 7.5 where T = Si + Ge, (e) crystallization temperature 140 °C, (f) 150 °C, (g) 175 °C, and (h) OSDA **4**.

Water content and OSDA/F content were other factors that seriously influenced the crystallization and kinetics of CIT-13. For water content, in this work, gel $H_2O/T$ ratios from 7.5 to 15 were tested. Within the studied range of the water content, only CIT-13 phases were crystallized. Water content was closely related to the rate of formation. When the batches were not seeded, crystallization of CIT-13 was faster in gels with less amounts of water. The

summary and PXRD patterns are shown in Table B1 and Figure B3. The $H_2O/T = 7.5$ gel crystallized pure CIT-13 within 2 weeks, while the $H_2O/T = 15$ gel required 5 weeks to yield the product. Seeding the batches with as-make CIT-13 shortened the crystallization time by ca. 1 week, but did not affect the overall tendency. The concentration of $OSDA^+F^-$ ion-pair in gels was studied within a range of $0.50 < OSDA^+F^-/T < 0.75$. As shown in Figure B4, pure CIT-13 phases were obtained when $OSDA^+F^-/T < 0.625$. But further increase in OSDA concentration resulted in a formation of unknown impurity. The presence of seeds did not make a substantial influence on the rate of formation of CIT-13 in this series.

Temperature and types of ovens were parameters that affected the crystallization other than variables of gel compositions. Hydrothermal syntheses were conducted with four batches having the same reference gel composition at four different temperature (140, 150, 160, 175 °C) to investigate the influences of the crystallization temperatures. The PXRD profiles and SEM images of aliquots and final products from these trials are shown in Figures B5 and B6, respectively. The higher temperature the crystallization temperature was, the faster CIT-13 was formed. At 175 °C, pure CIT-13 was crystallized within a just week even without seeds; however, it took at least 4 weeks at a temperature below 150 °C. Also, the crystallization temperature influenced the size of product crystals. As shown in Figure B6, when a static-type oven was used, an increase in the crystallization temperature resulted in an increase in the crystal size. Agitation by using a rotary oven instead of a static oven also significantly influenced the crystal morphology (see Figure B7). From a static oven, large (> 20 μm) and apparently polycrystalline crystallites were obtained. When the batch was continuously agitated in the course of the crystallization, the size of crystallites was much smaller (~ 2–5 μm), and the crystallites had a single-sheet-like morphology. This difference is because the agitation of the batch influenced both nucleation and diffusion in the system by attenuating the concentration gradients of gel species and generating transport flows in gels, respectively.

The structure of the OSDA is a crucial variable that determines the resultant frameworks.[114] The Davis group reported the crystallization of germanosilicates using a series of imidazolium-derivative OSDAs having ortho-, meta-, and para-methylbenzyl pendant groups.[63] The OSDA having a methyl group on the ortho-position of the benzyl group crystallized an IWS-type germanosilicate when the Si/Ge ratio of gels was low (Si/Ge < 2), whereas the use of para-substituted benzylimidazolium derivative resulted in LTA-type germanosilicates, aluminosilicates, and pure-silica LTA.[62-63] Only the methyl-substituted configurational isomer (1,2-dimethyl-3-(3-methylbenzyl)imidazolium) yielded pure CIT-13 phases in a wide range of Si/Ge ratios.[63] In this work, four related imidazolium-derivative cations (**1**, **2**, **3**, and **4**) having one or two methyl groups on the meta- site of their benzyl rings are tested in the germanosilicate system of Si/Ge ratios from 2 to 16. The structures are shown in Figure 6.2, and the resultant XRD profiles taken every week are provided in the Appendix B (Table B1, Figures B8, B9, and B10).

The diffraction peaks corresponding to CIT-13 are observed in batches containing any of the four OSDAs when Si/Ge < 16. However, only OSDA **1** and OSDA **4** successfully crystallized pure CIT-13 phases within a reasonably wide range of Si/Ge ratios. In batches of OSDA **2**, an MFI impurity phase was observed, and this impurity MFI phase dominated the product mixture when the Si/Ge ratio is high (Figure B8). Several previous works described the inclusion of Ge within the MFI framework,[171, 192] but it was unclear whether Ge was incorporated in the MFI impurity phase observed in this work. OSDA **3** also yielded CIT-13 but one or more unidentified impurity phases were observed at all gel Si/Ge ratios (Figure B9).

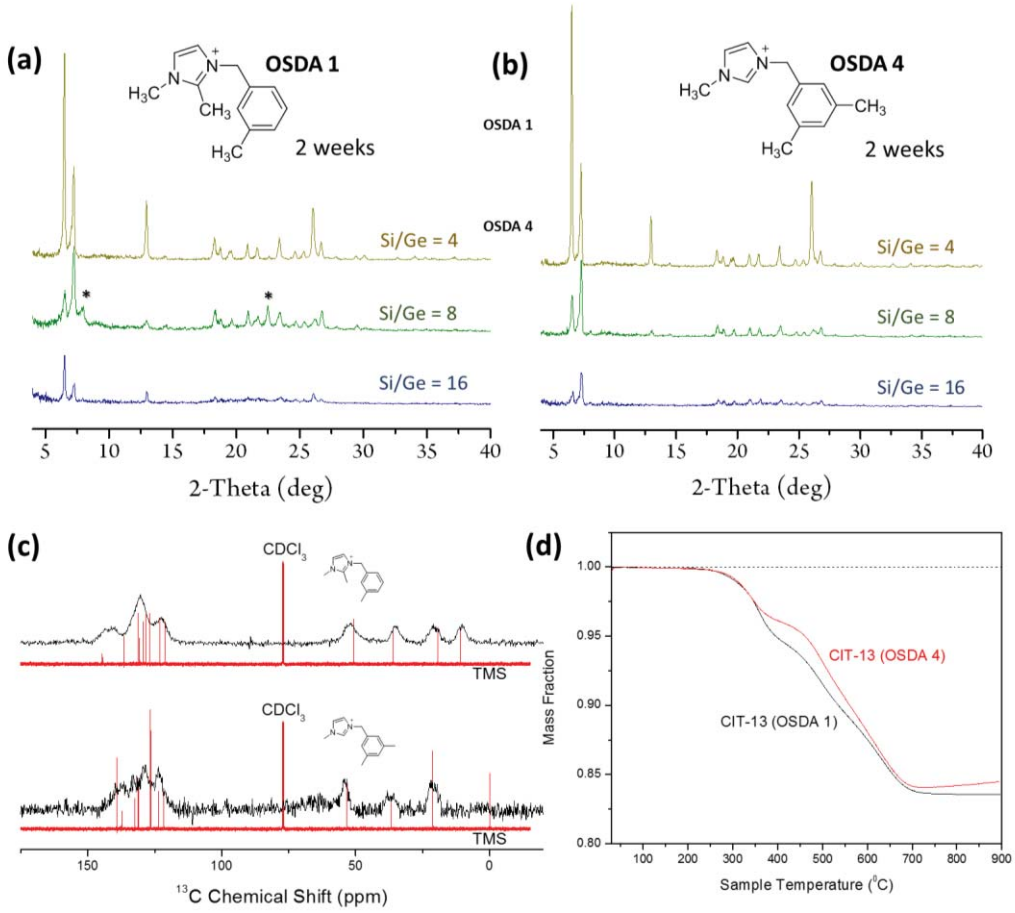


Figure 6.5. PXRD profiles of the samples crystallized from different Si/Ge ratios in the gel with (a) OSDA 1 and (b) OSDA 4 for gel compositions x/(1+x) $SiO_2$ : 1/(1+x) $GeO_2$ : 0.5 ROH : 0.5 HF : 10 $H_2O$. (x is the Si/Ge ratio of gels; Asterisks * denote impurity peaks.) (c) $^{13}C$ solid-state 8 k MAS NMR spectra (black) of as-made CIT-13 from OSDA 1 and OSDA 4, overlapped with the $^{13}C$ solution (in $CDCl_3$) NMR spectra (red) of the corresponding OSDAs. (d) TGA profiles of as-made CIT-13 samples from OSDA 1 and OSDA 4.

OSDA **1** and OSDA **4** yielded high-purity CIT-13 germanosilicates with little impurity within 2 weeks at gel Si/Ge = 4, 8, and 16. Figure 6.5(a) and 6.5(b) show the PXRD patterns of products after 2 weeks of crystallization with OSDA **1** and OSDA **4**. For both OSDAs, the crystallinities were better when gel Si/Ge ratios were low. Also, the OSDA molecules were occluded within the pore systems of CIT-13 without degradation. The $^{1}$H-decoupled $^{13}$C solid-state 8 k MAS NMR spectra of as-prepared CIT-13 from the two OSDAs matched well with the $^{13}$C solution NMR spectra of the two OSDAs in $CDCl_3$. (Figure 6.5(c)) From the TGA profiles of as-prepared CIT-13, the weight fractions of OSDA molecules in as-prepared molecular sieves can be estimated. From the weight losses of TGA profiles shown in Figure 6.5(d), it was calculated that OSDA **1** and OSDA **4** occupied 16.5% and 15.6% of as-prepared CIT-13, respectively. If a unit cell of as-prepared CIT-13 had contained 4 OSDA molecules, the weight loss of TGA should have been 18%. However, the estimated values were lower than that. The structure refinement based on the synchrotron X-ray diffraction of as-prepared CIT-13 revealed that the OSDA occupancy was less than unity (ca. 0.8), which is corresponding to a weight loss of 15%. This incomplete OSDA occupancy is probably a result of the disorder in the *d*4*r* unit arrangement in the CIT-13 framework. Similar types of reduced occupancy were also observed in the case of SSZ-55 (ATS) and SSZ-59 (SFN).[172]

CIT-13 could be synthesized using $NH_4F$ instead of concentrated HF solution. Replacing HF with $NH_4F$ is important in terms of scaled-up industrial production since it provides a way to avoid the use of volatile and dangerous HF. It was proven that equimolar amounts of $NH_4F$ can replace HF successfully, yielding identical CIT-13 products. Two CIT-13 samples, one from the reference condition using HF and the other from a protocol that used an equimolar amount of $NH_4F$ instead of HF, were prepared in an 160 °C static oven and compared with PXRD, SEM, EDS, TGA, and Ar-adsorption at 87.45 K. The PXRD profiles agreed to each other without impurity peaks (Figure 6.6(a)). The SEM micrographs shown in Figure 6.6(b) and 6.6(c) demonstrate that the two CIT-13 have very similar

morphology. From the TGA profiles given in Figure 6.6(d), it was found that the two as-prepared CIT-13 samples possessed very similar amounts (16.5 wt. % for CIT-13/HF and 16.1 wt.% for CIT-13/$NH_4F$) of occluded organic molecules. Finally, the Ar adsorption isotherms from freshly calcined versions of the two CIT-13 well matched each other (Figure 6.6(e)). The micropore volumes of CIT-13/$NH_4F$ characterized based on the t-plot model and the Saito-Foley (SF) model[173] were 0.191 $cm^3\ g^{-1}$ and 0.215 $cm^3\ g^{-1}$, respectively. These values are very close to the values obtained from CIT-13/HF (0.182 $cm^3\ g^{-1}$ from the t-plot method and 0.222 $cm^3\ g^{-1}$ for the SF model).

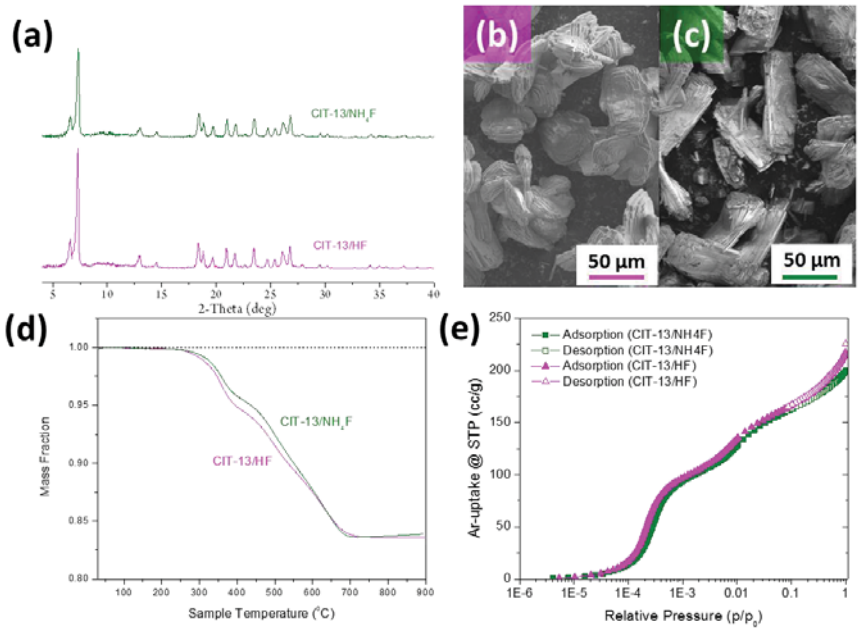


Figure 6.6. (a) PXRD profiles of as-prepared CIT-13 using $NH_4F$ (green) and HF (magenta) as the mineralizing fluoride sources. SEM images of CIT-13 resulting from the (b) HF and (c) $NH_4F$ protocols. (d) TGA profiles of as-prepared CIT-13 using $NH_4F$ (green) and HF (magenta). (e) Ar adsorption and desorption isotherms (log-scale, 87.45 K) of calcined CIT-13 from $NH_4F$- (green) and HF-protocol (magenta).

### *6.3.1.2. Aluminogermanosilicate System in Fluoride Media*

The incorporation of aluminum is investigated on the basis of aluminogermanosilicate ternary elemental compositions. Although it is known that germanium incorporated in germanosilicate framework shows a weak Lewis acidity,[142, 156] it is desirable to incorporate elements having an oxidation state of +3 (*e.g.*, B, Al, Ge. Fe, In, etc.) with a tetrahedral coordination in frameworks to let resultant molecular sieves have decent strength of Brønsted and Lewis acidities.[153, 173] Generally, there are two ways to incorporate these elements within germanosilicate frameworks: direct incorporation in hydrothermal synthesis and postsynthetic modification. In this section, the method of direct incorporation of aluminum in CIT-13 hydrothermal synthesis will be discussed. The postsynthetic method will be discussed in Chapter VIII.

The ternary gel elemental composition diagram and resultant phases are illustrated in Figure 6.7(a). Pure CIT-13 phases were obtained only when the Al-composition of gel was low (gel Si/Al < 20). A PXRD pattern of Al/Ge-CIT-13 obtained from a gel having a Si/Al ratio of 30 is compared with that of pure germanosilicate CIT-13 in Figure 6.7(b). With high aluminum contents (Gel Si/Al < 20) in gels, LTA phases were primarily obtained. This narrow tolerance for aluminum contents in the Si-Al-Ge CIT-13 ternary system resembled the Si-B-Ge and Si-Al-Ge UTL ternary systems in which STT or STF phases appeared with high boron or aluminum contents.[153, 1617] Inclusion of aluminum also resulted in smaller crystal sizes (SEM: Figure 6.7(e)) and longer crystallization times. This observation was also in consistent with an analogous study on UTL.[153]

The $^{29}$Si NMR of obtained Al/Ge-CIT-13 (Figure 6.7(c)) showed a broad peak in the range of -100 to -120 ppm. There are seven crystallographically different T-sites in the unit cell of CIT-13, and two heteroatoms (Al, Ge) which shift silicon signal toward downfield. Furthermore, the high bond strain of *d*4*r* units contribute to overlapping of peaks. The $^{27}$Al NMR spectrum of Al/Ge-CIT-13 is shown in Figure 6.7(d). Only one broad signal at 50.5

ppm, which corresponds to tetrahedral aluminum sites, was observed. This absence of octahedral aluminum species is also seen in the direct incorporation of aluminum in UTL.[153]

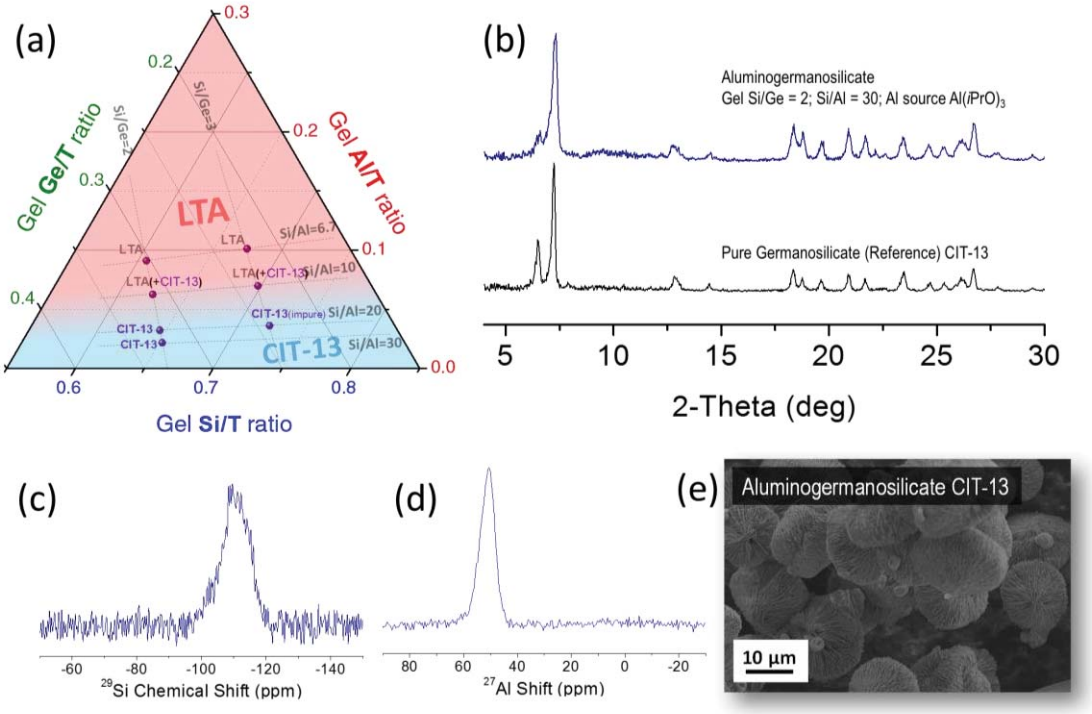


Figure 6.7. Material characterization results of Al/Ge CIT-13. (a) The resultant phases of hydrothermal products (T = 150–175 °C, for 1–4 weeks) denoted on a Si-Al-Ge ternary gel composition diagram. (b) PXRD pattern of Al/Ge-CIT-13. (c) 8 kHz MAS solid-state $^{29}$Si NMR spectrum of Al/Ge-CIT-13. (d) 12 kHz MAS solid-state $^{27}$Al NMR spectrum of Al/Ge-CIT-13. (e) SEM image of obtained Al/Ge-CIT-13 crystallites.

#### *6.3.1.3. Germanosilicate System in Hydroxide Media*

Ge-CIT-13 could be prepared without use of fluoride. Some other *d4r*-type germanosilicates such as ITQ-13 and ITQ-22 can be prepared from both fluoride-based and hydroxide-based recipes.[146, 175-176] IM-12 is also prepared without any fluoride media.[116]

The gel compositions for hydroxide-based CIT-13 syntheses trials are shown in Table B4. In this work, CIT-13 samples synthesized in hydroxide media were denoted as CIT-13/OH(#) where # is the sample number shown in Table B4. Also, only in contexts where comparisons between fluoride- and hydroxide-media were made, CIT-13 samples from fluoride media were denoted as CIT-13/F.

Figure 6.8 shows PXRD profiles, SEM images, $^{29}$Si NMR spectra, and argon adsorption isotherms (87.45 K) of several selected CIT-13/OH samples. PXRD patterns shown in Figure 6.8(a) are comparable to typical CIT-13/F PXRD patterns. The ortho-isomer (denoted "Ortho" in Table B4) of OSDA **1** which yields IWS-type germanosilicates in fluoride media[8] was also able to crystallize pure CIT-13 in hydroxide media. In this work, OSDA **1** was generally used to prepare CIT-13/OH samples.

The hydroxide-mineralized crystallization generally took longer than the cases of fluoride-based recipes. Although CIT-13/OH showed planar crystal morphologies similar to CIT-13/F, as shown in Figure 6.8(b) and (c), CIT-13/OH crystals were generally smaller than CIT-13/F crystals despite longer crystallization times. Example $^{29}$Si NMR spectra of CIT-13/OH and CIT-13/F are compared in Figure 6.8(d). Shapes of $^{29}$Si resonance patterns were very similar to each other. This result implies that the natures Si-sites in the CIT-13 framework were very similar regardless of type of mineralizers used. Further deconvolution of $^{29}$Si NMR spectra was not performed. An argon adsorption isotherm of CIT-13/OH was also obtained and compared to that of CIT-13/F. The CIT-13/OH isotherm also shows two-step adsorption at $p/p_0 = 5\times10^{-4}$ and 0.01 just like other CIT-13/F samples as shown in Figure 6.8(e). This two-step adsorption behavior will be discussed in detail in Section 6.3.3. The micropore volumes of CIT-13/OH estimated based on the t-plod method and the Saito-Foley (SF) model were 0.171 cc $g^{-1}$ and 0.202 cc $g^{-1}$, respectively.

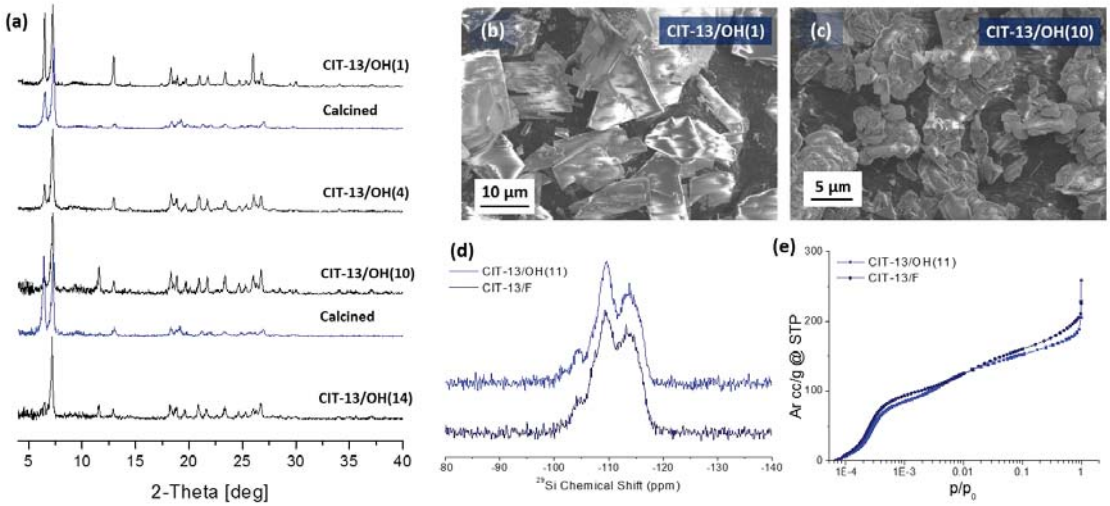


Figure 6.8. (a) Examples of PXRD patterns of CIT-13/OH samples. (b) SEM images of selected CIT-13/OH samples. (d) 8 kHz MAS $^{1}$H-decoupled $^{29}$Si solid-state NMR spectra of CIT-13/OH(11) compared to that of CIT-13/F. (e) Argon adsorption isotherms (87.45 K) of CIT-13/OH(11) and a typical CIT-13/F.

### 6.3.2. Structural Disorder within CIT-13

An in-depth structural study on as-prepared CIT-13 was performed in collaboration with Dr. Stef Smeets from Stockholm University, Sweden (now at TU Delft, the Netherlands) and Dr. Lynne B. McCusker from ETH Zürich, Switzerland.

The Rietveld refinement of as-prepared CIT-13 was performed based on the PXRD using a synchrotron beamline. The observed and calculated 1-dimensional patterns are shown in Figure 6.9. The crystallographic information calculated from the refined model is given in Appendix B. Due to the presence of OSDA molecules filling up the channel system, the refinement was performed at a lower symmetry $P\bar{1}$. (The original model determined based on the rotational electron diffraction (RED) experiment of calcined CIT-13 belongs to

the space group *Cmmm*.[63]) The main difference between the observed and calculated diffraction profiles (Figure 6.9.) is presumably due to the asymmetric peak shapes of the observed profile. A complete interpretation for this asymmetric peak shape was not made. The Si/Ge ratio of the refined model was 5.63 which matches well with the value observed using EDS (5.73±0.89). Also, most Ge atoms were located in the d4r units. The estimated occupancy of OSDA was 3.26 molecules per unit cell which is 81.5% of the full occupancy (4 molecules per unit cell). This incomplete occupancy also agrees well with the observed weight loss from the TGA experiment which is smaller than the expected value (*vide supra*). The positions of fluoride anions were located at the center of the *d*4*r* units, similarly to other germanosilicate frameworks possessing the *d*4*r* units synthesized from fluoride media.[21]

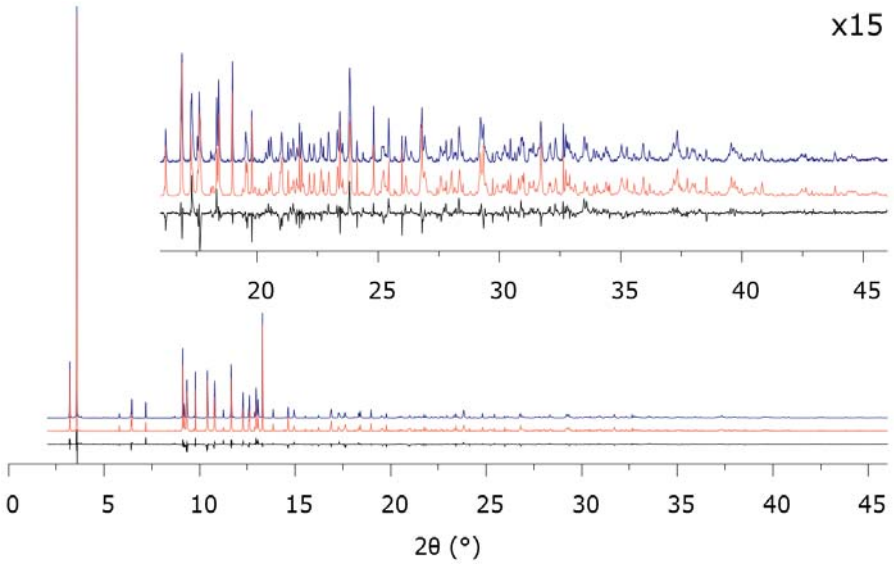


Figure 6.9. The observed diffraction profile (blue), calculated profile (red), and difference between the two (black) for the Rietveld refinement of as-prepared CIT-13.

The disorder in CIT-13 is originated from multiple number of possible arrangements of the *d*4*r* units in the framework. As previously mentioned, the CIT-13 framework is composed of the *cfi*-layers and the 2-dimensional arrays of *d*4*r* units connecting neighboring layers. There are two different ways to stack the *cfi*-layers: ABAB and AAAA as shown in Figure 6.10(a) and 10(b). The presence of this stacking disorder in CIT-13 is also suggested based on the high annular dark field scanning transmission electron microscopy (HADDF STEM).[165] No line broadening due to this type of disorder was observed in the powder diffraction pattern. This result suggests that CIT-13 consists of 10–20-unit-cell sized domains of either ABAB or AAAA along the x-axis.

Figures 6.10.(c) and (d) illustrate the other type of disorder which is related to the arrangements of *d*4*r* units *within* the interlayer region. One possible arrangement shown in Figure 6.10(c) generates straight 10-ring channels, while the other displayed in Figure 6.10(d) makes the 10-ring channels sinusoidal. However, the staggered arrangement of *d*4*r* units (Figure 6.10(d)) makes the OSDA molecules arranged within the channel system of CIT-13 very unfavorable; the intermolecular distances among OSDA molecules are too close to or too far from their neighboring molecules, and the distances between the framework wall and molecules are also too close. Thus, it can be concluded that the staggered arrangement is less likely than the parallel arrangement shown in Figure 6.10(c).

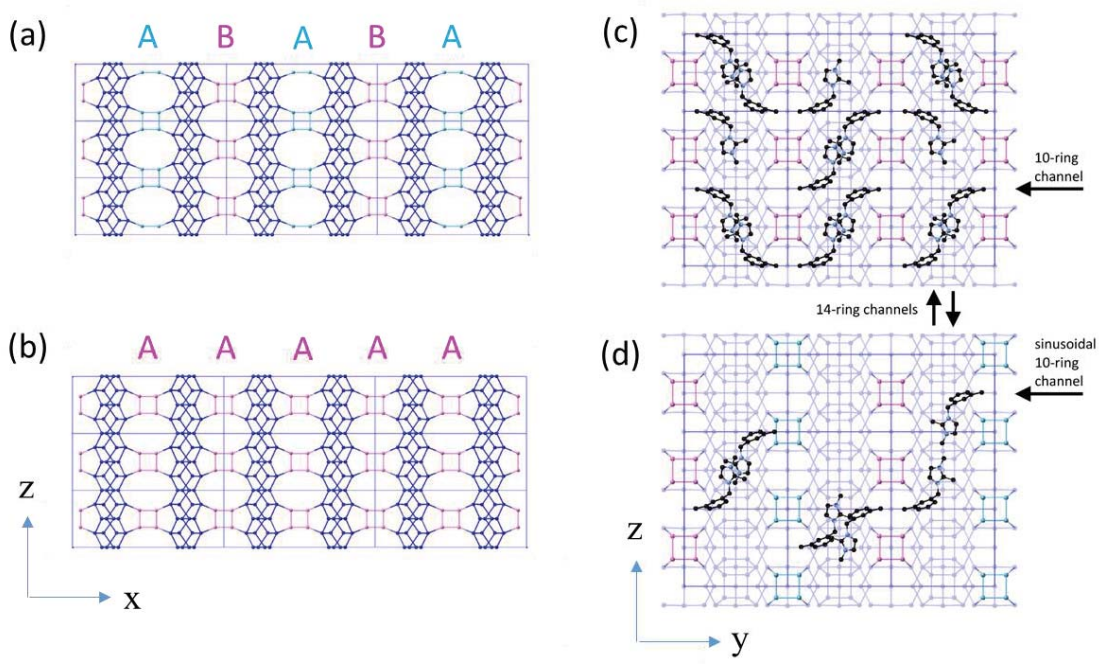


Figure 6.10. Schematic illustrations of possible disordered models for CIT-13. (a–b) Views along the y-axis showing two possibilities of the *cfi*-layers stacking mode: (a) ABAB and (b) AAAA. (c–d) Projections along the x-axis showing two possibilities of the *d*4*r* unit arrangements together with OSDA molecules within the interlayer region making (c) straight 10-ring channels and (d) tortuous 10-ring channels.

### 6.3.3. Comparison to Relative Germanosilicates

The UTL-type germanosilicate is another framework that is composed of Si-rich dense layers and 2-dimensional arrays of Ge-rich *d*4*r* units, belonging to a monoclinic space group *C2/m*. The *fer*-layers are interconnected with the *d*4*r* units and an extra-large pore channel system consists of perpendicularly intersecting 14-ring and 12-ring straight channels are present within the interlayer region. Due to the structural difference between *fer*-type layers and *cfi*-type layers, the UTL framework has no disorder within the interlayer region

that is the case for CIT-13. The schematic illustrations which demonstrate similarities and differences between UTL and CIT-13 are provided in Figure 6.11.

A high-Ge extra-large pore molecular sieve IM-12 having a UTL topology was prepared and compared to CIT-13. IM-12 was synthesized using a spiro-type ammonium OSDA, (6R,10S)-6,10-dimethyl-5-azaspiro[4.5]decanium, in hydroxide medium according to the protocol reported previously in literature.[116] The PXRD profile and SEM image of the resultant as-prepared IM-12 is shown in Appendix (Figure B11). The Si/Ge ratio of the IM-12 was 4.5 which is lower than that of the compared CIT-13 (Si/Ge = 5.0).

The $^{29}$Si solid-state NMR spectra of freshly calcined two germanosilicates are shown in Figure 6.12(a). Signals were almost absent in the region -100 to -105 ppm. Thus, these two germanosilicates had almost no significant $Q^3$ silanol groups and could be regarded as complete *tecto*-germanosilicates. For both germanosilicates, multiple peaks which significantly overlap with one another were observed in the region -105 to -120 ppm. IM-12 showed more peaks than CIT-13, probably because the framework UTL has more crystallographically unique T-atoms (twelve) than CIT-13 (seven). The signals within the region -110 to -120 ppm are contributed by high silica $Q^4$-Si atoms residing in *fer*- or *cfi*-layers.[118] Small shoulder signals observed in the region -105 to -110 ppm must be either $Q^4$-Si atoms in the *d*4*r* units[154, 177] or Si atoms neighboring with one or more Ge atoms,[153, 178] but conclusive peak assignments were not made here.

The micropore volumes of IM-12 and CIT-13 were obtained based on Ar adsorption isotherms at 87.45 K. Based on the t-plot method and the Saito-Foley model, the estimated micropore volumes of IM-12 were 0.177 $cm^3\ g^{-1}$ and 0.205 $cm^3\ g^{-1}$. The acquired isotherms described in linear scale and logarithmic scale are demonstrated in Figure 6.12.(b) and (c). Unlike IM-12, CIT-13 showed a characteristic two distinct steps of pore filling phenomena which is apparent in the log-scale chart shown in Figure 6.12.(c). The first pore filling occurred at $p/p_0 \sim 10^{-4} – 10^{-3}$ and the second pore filling appeared at $p/p_0 \sim 10^{-2}$. The former

may be contributed to pore-filling of the narrow and eccentric 10-ring channels and the latter may be from pore-filling of remaining space within the wide 14-ring channels. The pore-size distribution derived from the isotherm of CIT-13 based on the cylindrical Saito-Foley model[173] is shown in Figure B12(a). Unlike IM-12, CIT-13 apparently shows a two-step pore-filling behavior. The reason why IM-12 did not show such behavior may be that the 12-ring channel of IM-12 has no high eccentricity and a size close to that of the 14-ring main channel of UTL. Argon isotherms of zeolite A (LTA) and Y (FAU) are provided in Figures B12(b) and (c) for clearer comparison.

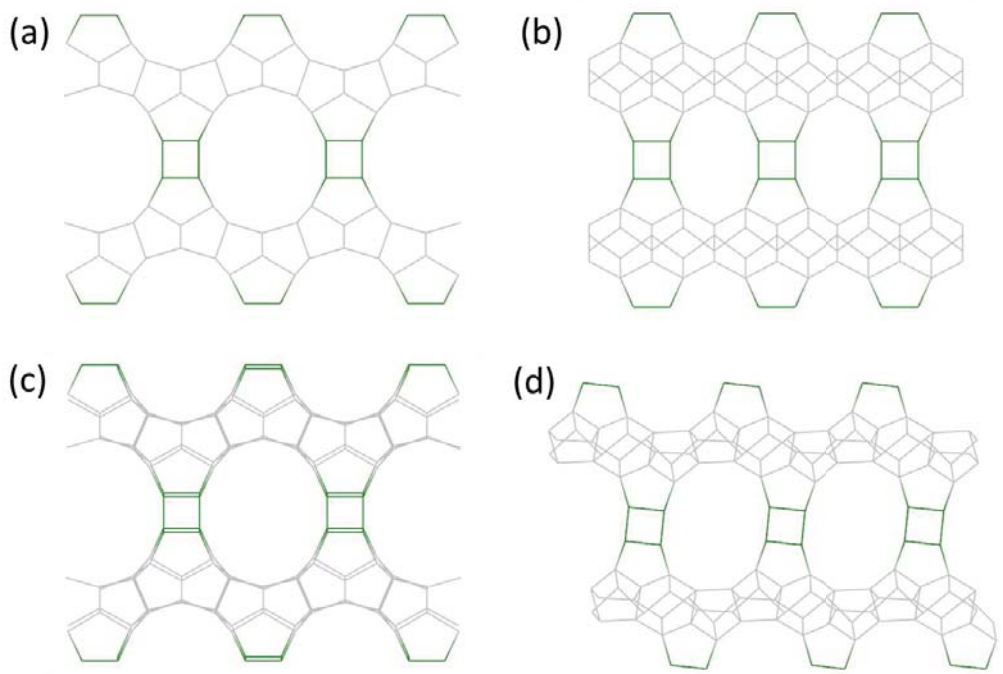


Figure 6.11. Comparison between the crystal structures of CIT-13 and IM-12. (a) CIT-13 viewed along the [001] direction showing the 14-ring pore, and (b) along the [010] direction showing the 10-ring pore. (c) IM-12 viewed along the [001] direction showing the 14-ring pore, and (d) along the [010] direction showing the 12-ring pore.

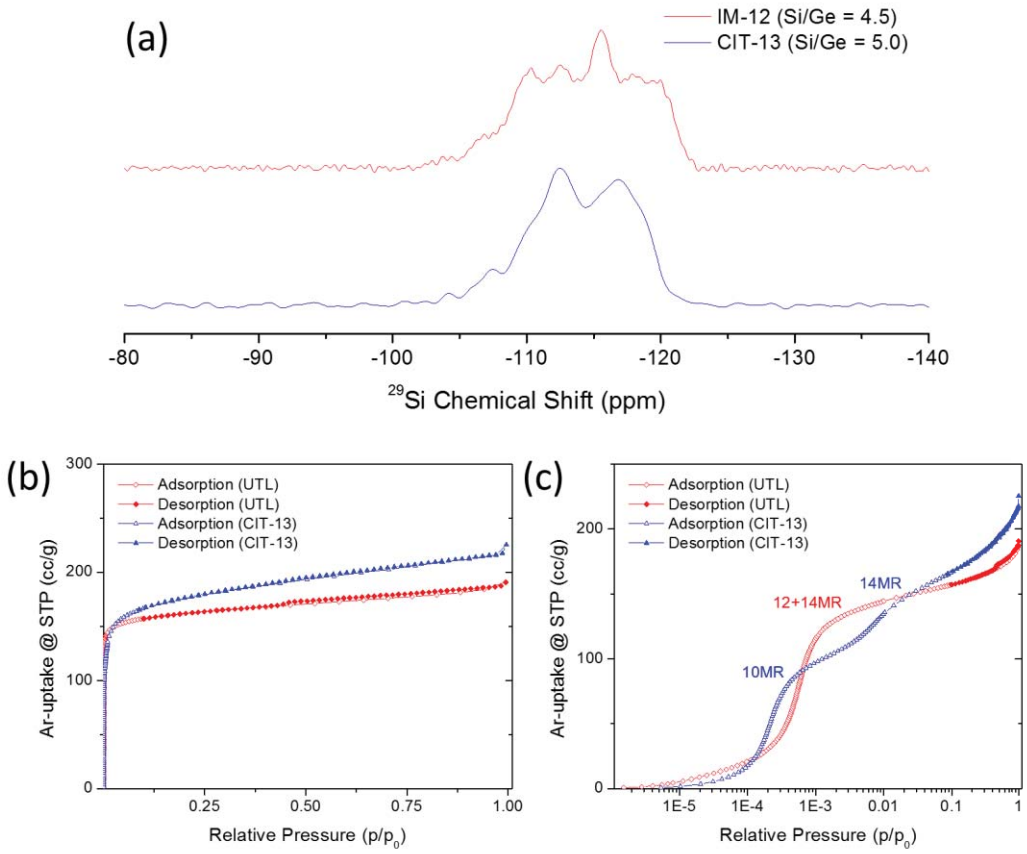


Figure 6.12. Material characterization results of IM-12 and CIT-13. (a) $^{1}$H-decoupled $^{29}$Si solid-state 8 k NMR spectra of IM-12 and CIT-13. Ar adsorption and desorption isotherms at 87.45 K of IM-12 and CIT-13 in (b) linear and (c) log-scale.

## 6.4. Summary

In this chapter, the synthesis conditions for CIT-13 were optimized. The gel composition of 0.80 $SiO_2$ : 0.20 $GeO_2$ : 0.5 ROH : 0.5 HF : 10 $H_2O$ was suggested as the optimized synthesis condition for CIT-13 in fluoride media. It was experimentally shown that HF can be replaced with the same molar amount of ammonium fluoride. For

isomorphous substitution synthesis, the ternary gel system of Al, Ge, and Si was studied. LTA phase appeared as the major impurity phase when the gel Si/Al ratio was low (Si/Al < 20). CIT-13 could be also synthesized without fluoride. The CIT-13 sample synthesized in hydroxide media showed properties similar to CIT-13 from fluoride-mediated syntheses. The nature of structural disorder was also studied on the basis of the Rietveld refinement result, focusing on the arrangement of *d*4*r* units within the interlayer region. It was concluded that the staggered arrangement of *d*4*r* units along the 10-ring direction is not favorable. Lastly, the properties of CIT-13 were compared to those of IM-12. CIT-13 showed a two-step argon adsorption behavior which may originate from the eccentricity of 10-ring pore which IM-12 does not have.